Advanced Functional Materials

ADVANCED FUNCTIONAL MATERIALS
www.afm-journal.de

RESEARCH ARTICLE

Strain-Engineered Gradient-Modulus Platforms for Mechanically Robust and Conformable Hybrid Electronics

Xiaojun Pan[1,2] | Zhangsheng Xu[2] | Yepei Mo[1,2] | Jiaqi He[2] | Jiaqi Tang[1,2] | Siyuan Wang[1] | Xingang Pan[3] | Zhiwei Fu[3] | Yanqi Gu[4] | Weidong Chen[1] | Wenchao Gao[2] | Rongrong Bao[1] | Caofeng Pan[1]

[1]Institute of Atomic Manufacturing, Beihang University, Beijing, P. R. China | [2]Beijing Institute of Nanoenergy and Nanosystems, Chinese Academy of Sciences, Beijing, P. R. China | [3]Xuzhou B&C Chemical Co. Ltd., Jiangsu, P. R. China | [4]National Key Laboratory of Science and Technology on Aero-Engine Aero-Thermodynamics, Research Institute of Aero-Engine, Beihang University, Beijing, P. R. China

Correspondence: Wenchao Gao (gaowenchao@binn.cas.cn) | Rongrong Bao (baorongrong@buaa.edu.cn) | Caofeng Pan (pancaofeng@buaa.edu.cn)

Received: 11 December 2025 | **Revised:** 27 January 2026 | **Accepted:** 21 February 2026

Keywords: rigid-flexible integration | strain-engineered substrate | stretchable electrodes | stretchable hybrid electronics | wearable electronic skin

ABSTRACT

Stretchable hybrid electronics offer a compelling pathway for integrating rigid microelectronic components within soft, deformable platforms, crucial for the development of next-generation wearable and epidermal devices. However, the pronounced mechanical mismatch at the interface between stiff components and elastomeric substrates often leads to interfacial failure, including delamination and cracking, under dynamic strain conditions. In this study, we present a mechanically optimized and electrically resilient stretchable hybrid electronic system by co-designing substrate mechanics and conductive architectures. A photolithographically defined gradient crosslinking technique is utilized to fabricate a modulus-graded polydimethylsiloxane (PDMS) substrate, exhibiting a spatially tunable elastic modulus ranging from 0.12 to 1.4 MPa. This gradient-modulus configuration enables effective redistribution of localized strain, thereby alleviating stress concentration and enhancing mechanical durability at heterogeneous interfaces. Concurrently, a silver-PDMS composite conductor is developed, achieving high conductivity (1 Ω/sq under 50% strain), excellent stretchability, and environmental robustness. Direct-ink-writing using an inkjet platform facilitates precise patterning of conductive traces, allowing seamless integration of multifunctional sensor arrays capable of real-time monitoring of wrist kinematics and complex finger movements. This work underscores the synergistic integration of gradient mechanical engineering and scalable microfabrication strategies, paving the way for robust, high-fidelity wearable electronics and electronic skin systems.

1 | Introduction

Stretchable hybrid electronic devices are developed using a heterogeneous integration strategy that combines two essential attributes: mechanical deformability and high-fidelity signal transmission. This is achieved by synergistically integrating stretchable conductors with rigid functional components, including surface-mount devices (SMDs), printed circuit boards (PCBs), and flexible flat cable (FFC) connectors [1–3]. The resulting system unites the elastic mechanical behavior of soft substrates with the precise electrical performance of rigid elements. Such hybrid configurations offer promising prospects in a wide range of emerging applications, particularly in wearable health monitoring systems [4–7], implantable medical electronics, bionic tactile interfaces [8–10], and soft robotic actuation platforms [11–14]. Despite notable progress in the development of stretchable conductors and flexible substrates, the robust integration of rigid and soft materials remains a critical challenge, often limiting system reliability [15–17]. The primary difficulty lies in the risk of fracture failure due to the large modulus mismatch at

the interface between the rigid component and the stretchable substrate. This challenge underscores the need to implement effective strain-isolation strategies during integration to ensure stable operation in stretchable electronic systems.

To address the modulus mismatch at rigid-flexible interfaces, a strain-engineered substrate design strategy has been developed. This approach involves constructing stretchable substrates composed of predefined strain-free regions and strain-bearing regions [18, 19]. By introducing controlled gradients in material compliance, these architectures autonomously redistribute applied mechanical strains during deformation. Rigid components are embedded within strain-free "rigid islands," which are interconnected by stretchable conductors. When external strain is applied, mechanical stress is concentrated within the stretchable interconnects, while the rigid islands remain mechanically isolated, preserving their structural and electrical integrity throughout deformation. This strategy significantly improves the mechanical reliability of rigid components and mitigates failure risks under tensile loading [20]. Strain-engineered substrates achieve this functionality through spatial optimization of thickness profiles and Young's modulus gradients [21]. Current approaches to fabricating these substrates fall into three general categories, based on structural design and material uniformity: (1) spatially patterned geometries, (2) rigid-soft composite systems, and (3) substrates with intrinsic modulus gradients. In the first strategy, researchers employ microstructure surface patterning, such as periodic microgroove arrays, to induce local strain concentration [22–24]. Under deformation, thinner groove regions absorb most of the mechanical stress, while protruding areas experience minimal strain. Although this method effectively guides strain distribution, the resulting structural anisotropy limits isotropic stretchability. Furthermore, the reliance on inverted molds restricts scalability and design flexibility. The second approach involves rigid-soft composite architectures, in which high-modulus materials are embedded in low-modulus elastic substrates [25, 26]. This significant modulus mismatch is leveraged to create localized low-strain regions. However, this sharp contrast in mechanical properties can create significant interfacial stress concentrations, often leading to delamination or interface fracture during repeated loading cycles. In addition, multilayer isolation strategies are also widely utilized in stretchable electronic systems to mitigate the strain transferred to rigid components by stacking materials with varying mechanical properties [27–29]. While such designs can effectively decouple deformation, the presence of discrete interfaces between layers often leads to interfacial stress accumulation during large or cyclic loading. Furthermore, multilayer structures require precise alignment and sophisticated fabrication protocols, which can introduce structural inhomogeneity and diminish long-term mechanical reliability. A more integrated strategy involves intrinsic modulus modulation within a homogeneous substrate [30]. Through spatially controlled chemical modification, a gradient crosslinking network is formed, giving rise to localized stiff regions in situ [31, 32]. This approach maintains chemical continuity between the rigid zones and the soft matrix, thereby minimizing interfacial stress concentrations that typically plague heterogeneous systems [33, 34]. The gradual transition in mechanical properties enables more uniform stress distribution, enhancing both the stretchability and mechanical durability of the device.

Stretchable conductors constitute the second critical element in strain-engineered systems, simultaneously providing reliable electrical interconnection between thin-film devices and efficient dissipation of localized mechanical strains. In such designs, rigid islands remain largely undeformed, while tensile loads are absorbed by compliant interconnects. This necessitates stretchable electrodes that preserve low electrical resistance under high-strain conditions while maintaining mechanical integrity. To address these demands, both structural and material-based strategies have been explored. Structural approaches employ engineered geometries such as serpentine traces, fractal patterns, and flexure-based layouts to transform rigid metallic films into stretchable formats [35, 36]. These designs leverage the inherently low sheet resistance and high carrier mobility of metals, while enhancing mechanical compliance through geometric deformation. However, achieving high stretchability often requires complex designs, which can elevate resistance and complicate fabrication processes. As a result, material-based approaches have gained prominence. Material-based strategies, by contrast, provide scalable alternatives and fall into two categories: intrinsically stretchable conductors and composite conductive materials [37]. Intrinsically stretchable materials, such as gallium-based liquid metals [38–41] and ionic gels [42], offer unique properties, including self-healing and retention of conductivity through dynamic chemical bonding networks [43]. Composite conductors, by contrast, consist of conductive fillers-such as nanoparticles [44], nanowires [45–48], or carbon-based materials embedded in elastic polymer matrices [49]. These systems enable strain-insensitive conductivity and can be tailored by carefully selecting filler type, concentration, and polymer composition. Furthermore, their compatibility with scalable fabrication techniques such as flexible lithography [50], transfer molding [51], and inkjet printing makes them highly suitable for integrating stretchable circuits into practical applications.

Here, we present a hybrid stretchable electronic system enabled by a strain-engineered substrate incorporating photochemically induced gradient cross-linking to modulate the local Young's modulus. A photochemically induced gradient crosslinking process is applied to benzophenone-modified polydimethylsiloxane (BP-PDMS). We induce spatial variations in cross-linking density, resulting in an eleven-fold gradient in Young's modulus variation across a single substrate. This modulus gradient effectively guides mechanical strain into designated compliant regions, thereby shielding rigid components from mechanical failure and preserving electrical stability during deformation. Electrodes fabricated on the strain-modulated substrate exhibit minimal contact resistance change before and after stretching, confirming that strain redistribution plays a key role in maintaining resistance stability. To realize a stretchable conductor compatible with this substrate, we developed a printable micro-nano composite ink by blending hydrophilic silver nanosheets with hydrophobic PDMS in an organic solvent. The resulting conductive network demonstrates high strain tolerance, with a relative resistance change ($\Delta R/R_0$) of only 0.4 under 50% tensile strain. The intrinsic viscoelasticity of the PDMS matrix promotes strong interfacial adhesion between the ink and the substrate, effectively preventing delamination during cyclic stretching. The inkjet printing process enables high-resolution electrode patterning, while the integration of rigid chips with stretchable interconnects yields fully functional elastic circuits. These hybrid systems are capable of real-time, multi-joint

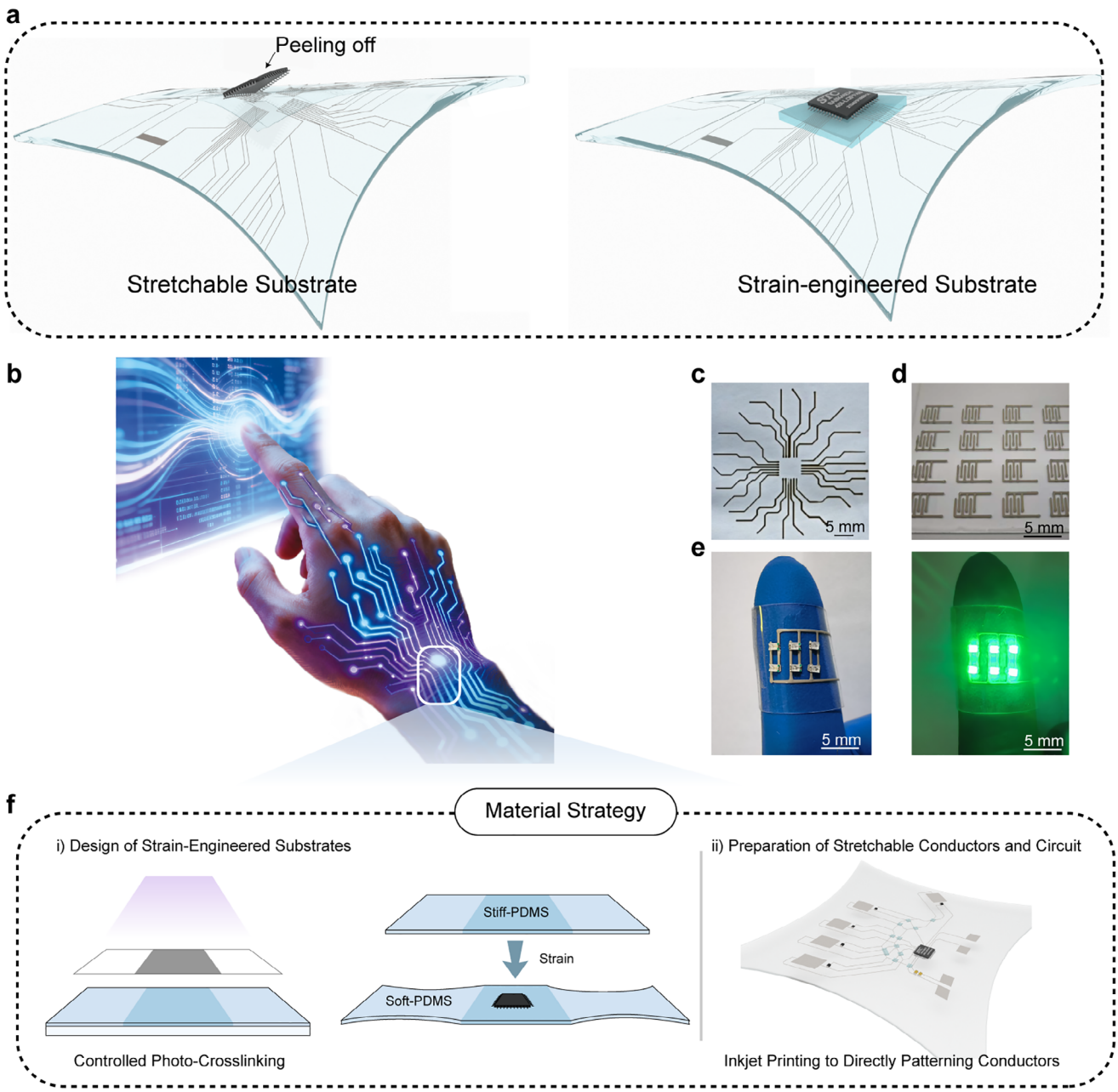

FIGURE 1 | Overview of the strain-engineered strategy for stretchable hybrid circuits. (a) Conventional substrates cause chip delamination, while strain-isolation substrates preserve stable chip-substrate connections. (b) Circuits conformally integrate on the hand, showing potential for human-machine interaction applications. (c–e) Printed stretchable electrodes enable versatile patterning and large-area array fabrication. (f) Materials strategy involving (i) strain-engineered substrate design and (ii) fabrication approach for stretchable conductors and circuit interconnects.

motion tracking and data transmission in human biomechanical monitoring. Taken together, this platform lays the groundwork for next-generation wearable electronics with clinical-grade motion sensing accuracy and long-term mechanical durability.

2 | Results and Discussion

Figure 1 summarizes the advantages and implementation of the strain-engineered strategy. Conventional substrates transfer external strain directly to the chips, leading to delamination, whereas strain-isolation substrates redistribute strain through modulus gradients, thereby preserving stable chip-substrate connections (Figure 1a). Circuits constructed with this strategy exhibit outstanding stability and reliability when conformally integrated on the hand, demonstrating strong potential for applications in human–machine interaction and related fields (Figure 1b). The stretchable electrodes are fully compatible with printing techniques, enabling versatile patterning and large-area array fabrication (Figure 1c,d), while enhancing the stability of integrated devices such as LEDs (Figure 1e). These performance advantages arise from two key fabrication steps. First, photomask-assisted crosslinking of benzophenone-functionalized PDMS produces patterned BP-PDMS substrates

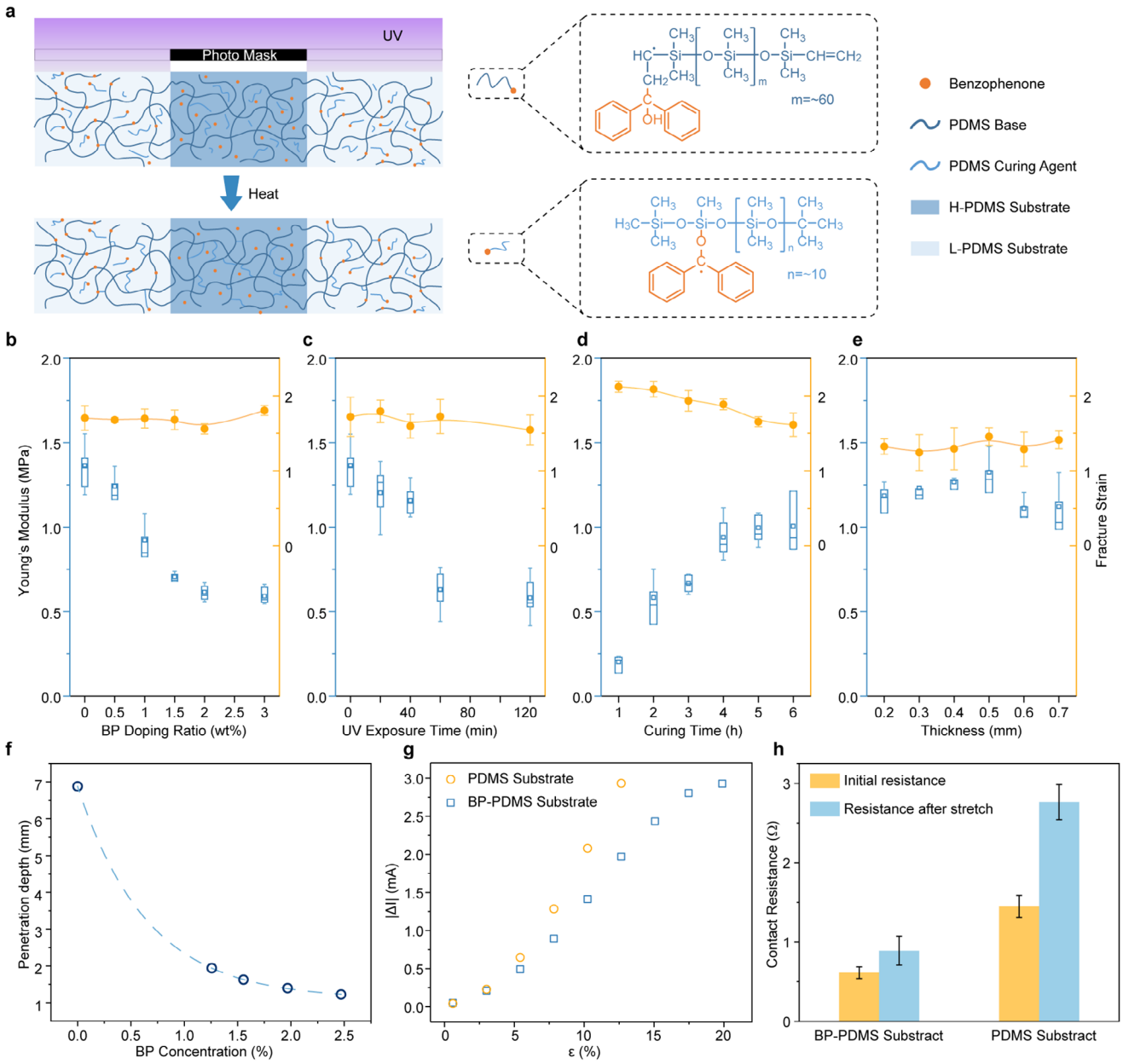

FIGURE 2 | Performance evaluation of strain-engineered stretchable substrates. (a) Schematic illustration of spatially controlled photo-crosslinking for constructing modulus-gradient architectures. (b–e) Young's modulus and fracture strain of BP-PDMS substrates as a function of (b) BP concentration, (c) UV exposure time, (d) thermal curing time, and (e) substrate thickness. (f) UV light (365 nm) penetration depth across varying BP concentrations, indicating tunable curing profiles. (g) LED current response under applied strain on substrates with and without strain-engineering treatment. (h) Contact resistance comparison before and after stretching for different substrate configurations.

with continuous modulus gradients to modulate strain distribution (Figure 1f-i). Second, conductive networks are formed by inkjet printing AgNPs-PDMS nanocomposites (Figure 1f-ii). Solvent-assisted dispersion and alignment of AgNPs promote uniform film formation and precise linewidth control, ensuring reliable electrical performance under strain.

2.1 | Design and Performance Characterisation of Strain-engineered Substrates

Figure 2 outlines the fabrication process of strain-engineered BP-PDMS substrates through spatially controlled photochemical cross-linking to generate modulus-gradient architectures. The substrates were prepared by uniformly mixing benzophenone (BP) photo initiator into a PDMS prepolymer matrix, followed by ultraviolet (UV) exposure through a patterned photomask to locally modulate cross-linking density (Figure 2a). Although multiple mechanisms have been proposed to explain the photo-crosslinking behavior of BP in PDMS systems, the prevailing model involves a redox reaction between siloxane moieties and the carbonyl groups of BP. Upon exposure to 365 nm UV light, BP undergoes photoactivation, generating reactive radical intermediates. These radicals disrupt the standard platinum-catalyzed hydrosilylation process by preferentially interacting with vinyl and Si—H bonds, thereby introducing a competing

radical pathway. This mechanism is schematically illustrated in Figure S1. In regions shielded from UV light by the photomask, the hydrosilylation reaction proceeds normally, forming long-chain cross-linked PDMS networks. In contrast, UV-exposed areas experience radical-mediated chain-transfer reactions that yield shorter, less cross-linked polymer structures. The truncated cross-linking in these regions inhibits further bonding between PDMS oligomers and curing agents, resulting in a significant reduction in local cross-linking density. This spatial differentiation in polymer network formation enables precise tuning of the Young's modulus within a single substrate. To verify the proposed reaction mechanism, Raman spectroscopy was conducted on BP-PDMS samples (Figure S2). UV-exposed regions displayed a distinct Si—H stretching vibration peak at 2160 cm^{-1}, which was markedly attenuated in thermally cured controls. This spectral signature supports the hypothesis that photoexcited BP preferentially abstracts hydrogen from Si—H bonds, thereby disrupting the cross-linking between vinyl and Si—H functionalities and validating the radical inhibition mechanism.

The tunability of Young's modulus in UV-exposed BP-PDMS substrates arises from the photochemical generation of benzophenone-derived radicals, which react with both vinyl and Si—H groups in the PDMS matrix, thereby inhibiting conventional cross-linking reactions. This mechanism enables precise modulation of mechanical properties by adjusting key processing parameters, including BP concentration, UV exposure time, thermal curing duration, and film thickness (Figure 2b–e). By systematically varying these parameters, the Young's modulus was tuned across a wide range, from 0.12 to 1.4 MPa, achieving an 11-fold difference while maintaining a strain at break exceeding 150%. The modulus modulation process is controlled by precise fabrication parameters, including exposure dose, photoinitiator concentration, and curing conditions, to ensure high reproducibility. Samples from multiple independent batches demonstrate highly consistent mechanical responses (Figure S3). These results indicate that the proposed fabrication strategy possesses excellent batch-to-batch uniformity and process stability, confirming its potential for scalable manufacturing. This mechanical performance is attributed to the radical-mediated inhibition of long-chain network formation, which selectively disrupts cross-linking without compromising the intrinsic chain entanglement of PDMS. As a result, modulus gradients are introduced while preserving the material's elasticity, offering a robust strategy for mechanical protection in hybrid stretchable electronics. Figure 2e further shows that the Young's modulus reaches a plateau around 1.2 MPa across different PDMS thicknesses, with negligible changes in strain at break. This observation suggests that within the studied thickness range, film thickness does not significantly affect UV penetration or radical generation. To quantify the relationship between film thickness, BP concentration, and UV absorption, we performed UV–vis spectroscopy measurements (Figure S4a). Based on the transmittance data and film thickness (Figure S4b), the penetration depth of 365 nm light was calculated for various BP concentrations (Figure 2f). Even at the highest BP concentrations, the minimum light penetration depth exceeded 1 mm, substantially greater than the maximum film thickness used in this study (500 μm). These results confirm that UV light can fully penetrate the films under all tested conditions, ensuring uniform radical generation and consistent modulation of cross-linking across the substrate.

We utilized finite element (FE) simulations to construct a simplified model of the strain-engineered substrate (Figure S5). Mechanistically, strain redistribution in substrates with a modulus gradient is governed by the spatial stiffness contrast. Within the elastic regime, regions with a lower Young's modulus preferentially accommodate the majority of the applied deformation, while high-modulus regions experience mechanical shielding. This behavior, characterized by the effective isolation of rigid components from external loads, is consistent with established studies on modulus gradients and strain isolation strategies. To assess the mechanical protection capabilities of the BP-PDMS substrate, we established an electromechanical testing platform that integrates commercial light-emitting diodes (LEDs) as strain-sensitive indicators (Figure 2g). From a fabrication perspective, the photomask-regulated photocuring process can realize continuous or stepwise modulus gradient distributions. However, for practical device design, we deliberately selected the two extreme modulus states corresponding to the UV-exposed and non-exposed regions to achieve a larger modulus contrast. This strategic choice strengthens the regulation of strain transfer pathways, thereby maximizing the protective effect on functional components. Devices fabricated on conventional PDMS and strain-engineered BP-PDMS substrates were subjected to incremental tensile strain, and the corresponding LED current was monitored in real time. Under low-strain conditions (≤3%), both substrates exhibited comparable electrical performance, as reflected by stable LED current levels. However, at strains exceeding this threshold, notable divergence emerged. In the case of conventional PDMS, electromechanical integrity deteriorated rapidly: the LED current dropped to 3 mA at 12% strain and subsequently exhibited irreversible electrical failure. This behavior reflects the substrate's inability to dissipate or redistribute mechanical stress, leading to localized strain accumulation at the interface between the rigid LED and the soft substrate, and ultimately causing mechanical and electrical failure. In contrast, devices based on BP-PDMS substrates demonstrated substantially enhanced strain tolerance. The spatial modulus gradient introduced by photochemical crosslinking effectively redirected mechanical strain away from the rigid LED region, thereby preserving interfacial integrity. Electrical functionality was sustained up to 20% strain without failure, indicating improved mechanical buffering and strain isolation at critical stress concentration points. These results confirm that BP-PDMS substrates significantly enhance the mechanical resilience of stretchable electronic systems by protecting rigid components from deformation-induced damage. The ability to engineer spatially graded mechanical properties within a single elastic substrate offers a viable route to prolonging device lifespan and improving system-level robustness in hybrid soft electronics.

Rigid-flexible interfacial mismatch is a critical factor contributing to delamination and failure in hybrid stretchable electronic systems. To further elucidate the stabilization mechanism at the rigid-soft interface, we conducted in situ contact resistance measurements under dynamic strain using a custom-built characterization setup (Figure S6). As expected, contact resistance increases with applied strain for both conventional and strain-engineered

substrates. This trend reflects the growing mechanical mismatch at the electrode-substrate interface during deformation. However, substrates incorporating strain-engineered modulus gradients exhibit a significantly smaller increase in contact resistance under the same strain conditions (Figure 2h). This reduced variation suggests that the spatially distributed Young's modulus enables autonomous redistribution of applied mechanical stress, effectively minimizing interfacial mismatch. This suppression of strain-induced resistance fluctuations underscores the key role of strain-engineered substrates in preserving interfacial electrical connectivity. By enabling autonomous redistribution of localized stress, the modulus gradient minimizes interfacial delamination and contact degradation, thus offering a robust material-level strategy to enhance interfacial stability and prolong device durability in stretchable hybrid electronic systems.

2.2 | Preparation and Characterization of Stretchable Conductors

Conductive materials used in stretchable electronic systems must sustain high electrical conductivity and robust interfacial adhesion under significant mechanical deformation. To meet these requirements, we developed a silver-PDMS (Ag-PDMS) composite conductor that integrates a conductive network within an elastic matrix. Micron-sized silver particles (~10 μm) were uniformly dispersed in PDMS prepolymer using 4-methyl-2-pentanone (MIBK) as a solvent, forming a stretchable conductor with a three-dimensional interpenetrating network (Figure 3a; Figure S7a). Surface characterization revealed a densely packed layer of silver particles, with hardly any exposure of the underlying PDMS. A portion of the silver was embedded in the PDMS substrate, promoting intense interfacial contact and reducing the risk of electrical discontinuities from exposed insulating regions. Cross-sectional imaging (Figure S7b) showed a continuous transition between the conductor and the BP-PDMS substrate, without a distinct physical interface. The deep infiltration of silver particles into the substrate facilitated the formation of a continuous three-dimensional percolation network. This interpenetrating architecture ensured both mechanical interlocking and chemical compatibility between the conductive phase and the elastomer substrate. Consequently, the composite conductor exhibited dual functional benefits: the interconnected silver network enabled stable charge transport under strain, while the strong mechanical and chemical integration with the PDMS substrate reduced interfacial delamination, enhancing the overall durability of the stretchable electrode.

By precisely adjusting the mass fraction of silver nanoparticles (Ag NPs) from 44 to 65 wt.%, we fabricated a series of stretchable conductors and systematically examined the correlation between their electrical properties and mechanical response (Figure 3b). All compositions demonstrated excellent initial conductivity, with sheet resistance values remaining below 0.35 Ω/sq and preserved their electrical performance both before and after mechanical deformation (Figure 3c). Resistance strain measurements (Figure S8) showed that conductors with higher Ag NP content (65 wt.%) exhibited minimal variation in resistance under strain ($\Delta R/R_0 < 4$ at $\varepsilon > 90\%$), indicating robust structural integrity and well-maintained conductive pathways. The Ag-PDMS composite maintains high conductivity under significant strain, a phenomenon largely attributed to the confinement effect exerted by the PDMS matrix on the silver fillers. Under mechanical deformation, the elastomeric matrix effectively constrains the migration and detachment of the fillers, thereby stabilizing interparticle contacts and preserving continuous conductive pathways. This confinement-regulated carrier transport mechanism substantially enhances the electromechanical stability of the composite, even under large-scale stretching [52–56]. This behavior suggests their effectiveness as stable electrodes in stretchable circuits, where consistent signal transmission under mechanical loading is essential. In comparison, conductors containing lower Ag NPs content (44 wt.%) displayed pronounced strain sensitivity, with a sharp increase in resistance under relatively small deformation ($\Delta R/R_0 > 40$ at $\varepsilon < 15\%$). This heightened electromechanical response renders them suitable for applications as sensing components that convert mechanical input into electrical signals. Notably, both types of conductors share an identical PDMS/Ag NPs composite matrix and differ solely in filler concentration. This intrinsic material compatibility enhances the interfacial adhesion and chemical affinity between the electrode and sensing layers, thereby improving the mechanical and electrical stability of the integrated device during repeated deformation cycles.

To further validate the application potential of the optimized stretchable conductor, we conducted a comprehensive performance evaluation of the composite containing 65 wt.% Ag NPs. Under dynamic tensile loading, the conductor maintained a stable resistance of approximately 1 Ω/sq at 50% strain (Figure 3d), highlighting its capacity to sustain high conductivity even under substantial mechanical deformation. To assess mechanical robustness under cyclic stress, we subjected the conductor to 10 000 stretching cycles at 40% strain (Figure 3e). Throughout the test, the relative resistance change remained within 0.5, with no signs of signal degradation or fatigue, indicating that the conductive percolation network remained structurally intact and functionally stable. Beyond uniaxial stretching, the electrical response of the electrodes was evaluated under torsional deformation. As illustrated in Figure S9, the electrode resistance remained stable while undergoing 180° torsion, which demonstrates reliable electrical performance under non-uniaxial strain conditions. In addition to mechanical resilience, the conductor demonstrated strong environmental durability. Immersion in phosphate-buffered saline (PBS), saline, and deionized water caused no observable delamination or surface degradation, and the normalized resistance (R/R_0) remained stable at ~1.5 (Figure 3f; Figure S10). Furthermore, the electrode's electrical performance remained consistent across a broad temperature range (25°C–95°C), with resistance variation confined within $R/R_0 < 1.8$ (Figure S11a). Moreover, while silver nanoparticles are inherently susceptible to oxidation, their encapsulation within the PDMS matrix minimizes direct exposure to ambient air. Consequently, the device continues to demonstrate stable electromechanical performance even after long-term storage in air, as the PDMS effectively functions as a protective barrier, as shown in Figure S11b. These results collectively underscore the chemical, thermal, and mechanical robustness of the 65 wt.% Ag NPs composites, making it a promising candidate for reliable operation in diverse and dynamic environments, such as in bioelectronic and wearable applications.

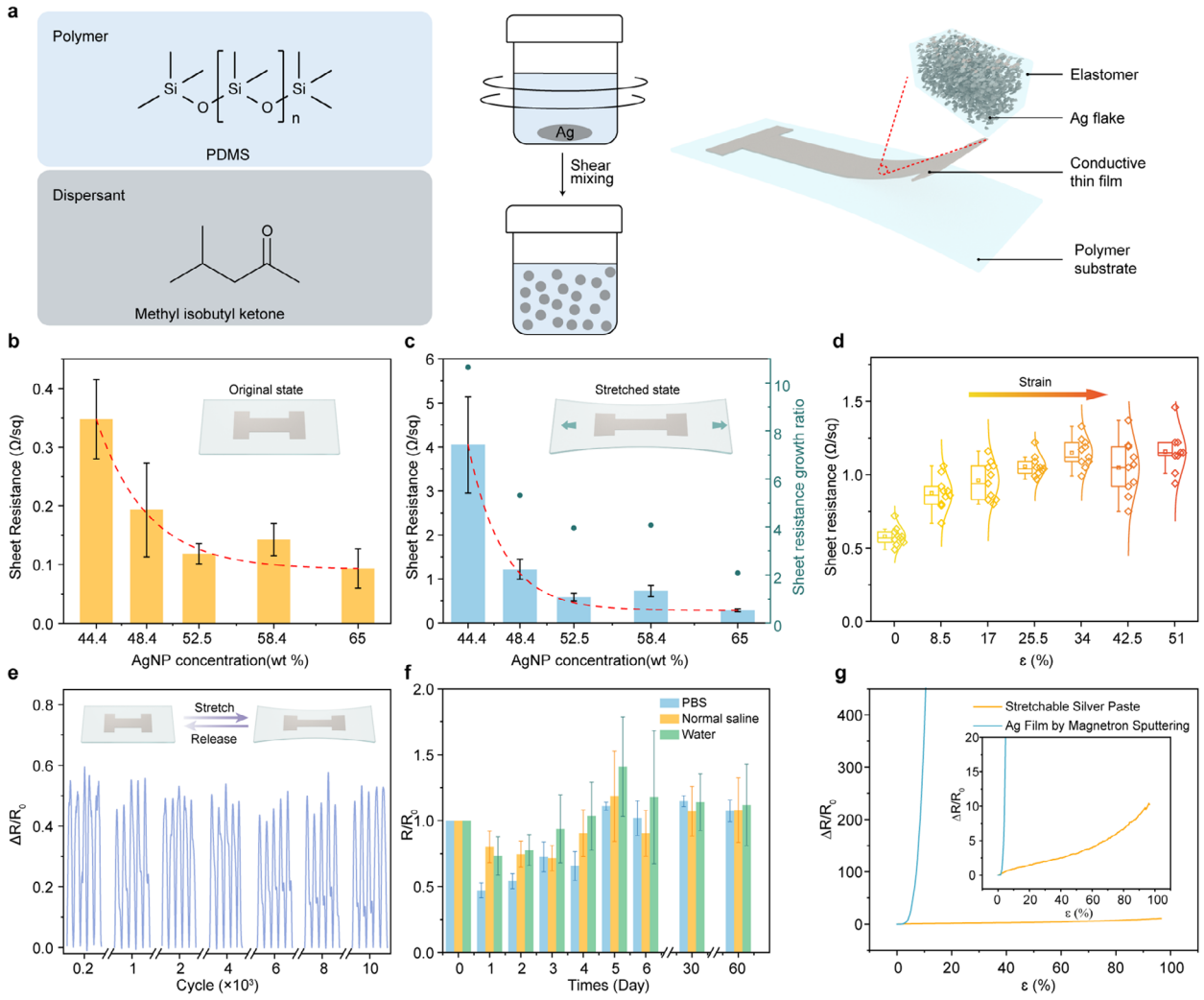

FIGURE 3 | Electromechanical performance of Ag-PDMS stretchable electrodes. (a) Schematic of the Ag-PDMS composite structure. (b) Sheet resistance of stretchable electrodes as a function of Ag particle concentration. (c) Square resistance of electrodes under 40% strain with varying Ag content. (d) Conductivity of stretchable electrodes with 65 wt.% Ag content under increasing strain. (e) Cyclic durability of Ag-PDMS electrodes under 10 000 cycles of 40% compressive strain. (f) Stability of Ag-PDMS electrodes immersed in different chemical environments. (g) Comparative performance between Ag–PDMS stretchable electrodes and magnetron-sputtered silver electrodes.

To evaluate the advantages of the developed stretchable conductor, its performance was systematically compared with that of conventional silver electrodes fabricated by magnetron sputtering. During chemical immersion tests, sputtered silver electrodes gradually detached from the substrate, leading to sharp increases in resistance and eventual electrical failure (Figure S12a). In contrast, the stretchable composite conductor exhibited stable electrical behavior and maintained strong adhesion, with no visible signs of delamination or structural degradation under the same conditions, highlighting its superior chemical stability. A dynamic washing test, designed to simulate mechanical agitation in aqueous environments (Figure S12b), further emphasized these differences. The sputtered electrode rapidly lost adhesion and failed electrically, whereas the composite conductor preserved its structural and electrical integrity throughout the process. Comparative resistance-strain measurements (Figure 3g) revealed a sharp increase in resistance ($\Delta R/R_0 > 400$) in the sputtered electrode at 10% strain. By contrast, the stretchable conductor maintained a low, stable resistance even under strains up to 100%, confirming its ability to maintain electrical functionality under substantial mechanical deformation. Adhesion testing (Figure S13) indicated that mechanical failure occurred within the conductor material itself rather than at the conductor-substrate interface, suggesting the formation of strong interfacial bonding between the conductor and the PDMS substrate. Moreover, stress-strain characterization (Figure S14) showed that the integration of the conductor did not alter the Young's modulus of the substrate. This result confirms that the conductor can be incorporated without compromising the mechanical compliance of the system, an essential attribute for maintaining the intended strain distribution and ensuring reliable device operation.

2.3 | Design and Application of Stretchable Circuit

To achieve high-precision integration of stretchable conductors within complex circuit layouts, we employed direct-ink-writing

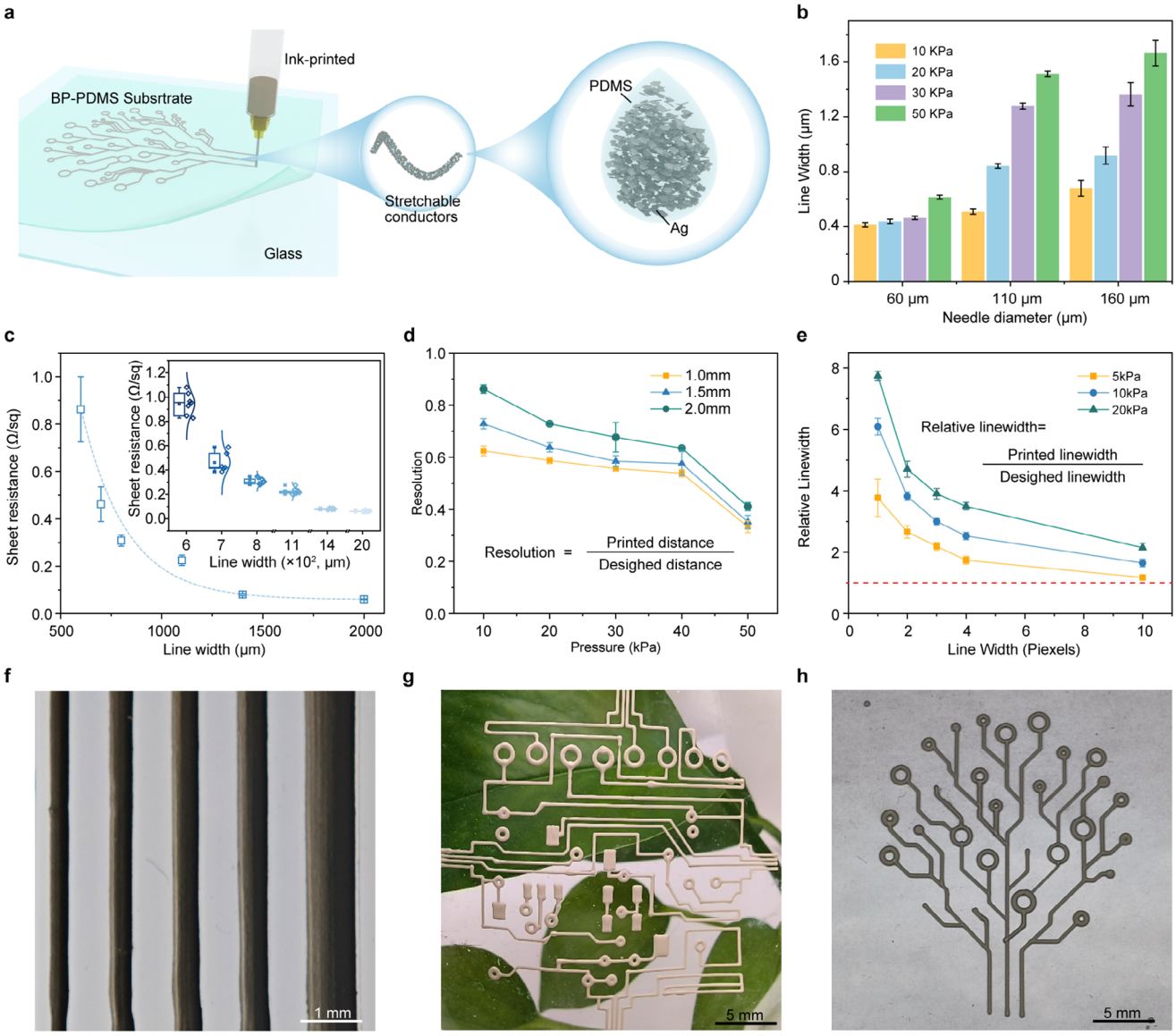

FIGURE 4 | Process optimization for inkjet-printed stretchable Ag-PDMS electrodes. (a) Schematic illustration of fabricating stretchable electronics by inkjet-printing Ag-PDMS conductive ink onto a PDMS substrate. (b) Average line width under different needle diameters (60–160 μm) and pressures (10–50 kPa). (c) Electrical conductivity of printed lines with varying linewidths. (d) Patterning resolution achieved under different printing pressures. (e) Normalized linewidths of printed traces as a function of injection pressure. (f–h) Optical images of representative printed Ag-PDMS traces demonstrating printing quality and uniformity.

(DIW) using an inkjet platform to directly pattern Ag-PDMS composite conductors (Figure 4a). DIW facilitates uniform dispersion and a preferential alignment of silver fillers within the PDMS matrix. As previously reported, this type of microstructural organization is beneficial for stabilizing conductive pathways and enhancing the electrical response of flexible electronic systems [57–60]. These structural features likely contribute to the stable and sensitive performance observed in this study. Key printing parameters were systematically optimized to ensure both functional reliability and compatibility with large-area fabrication. By adjusting nozzle diameters (ranging from 60 to 200 μm) and applied pressures (from 10 to 50 kPa), and analyzing the resulting printed structures, we fabricated stretchable conductor lines with widths between 500 μm and 2000 μm (Figure 4b). Due to the inherent fluidity of the composite ink, the printed features were typically wider than their designed dimensions. To achieve high patterning fidelity, the line width was finely tuned through precise control of jetting pressure and nozzle size. Given that the conductor width directly affects electrical performance, we evaluated the resistance of lines with varying widths. All printed lines exhibited excellent conductivity. In particular, lines with a width of 500 μm demonstrated a stable line resistance of approximately 1 Ω/cm (Figure 4c), along with consistent resistance-strain behavior under tensile deformation (Figure S15). To quantify printing precision, we defined resolution as the ratio of the actual spacing to the designed spacing between adjacent lines. A resolution approaching 1 reflects high patterning accuracy. Using a 60 μm nozzle, we printed line arrays under varying pressures and evaluated resolution quantitatively (Figure 4d). Due to droplet spreading during deposition,

the actual spacing was consistently smaller than the designed spacing, resulting in resolution values below 1. As printing pressure increased, resolution decreased steadily, attributed to the higher droplet ejection rate at higher pressures. This led to increased ink deposition per unit time and consequently greater lateral spreading, reducing the spacing between lines. Although lowering the pressure improves resolution, excessively low values (below 10 kPa) compromise the stability of ink delivery (Figure S16). In addition to resolution, we introduced relative linewidth as an indicator of patterning fidelity, defined as the ratio of the printed to the designed line width. A value close to one suggests accurate dimensional control. For narrow design widths (e.g., 60 μm), the printed lines were significantly wider than intended, yielding relative linewidths well above 1. As the design width increased, the relative linewidth gradually approached unity (Figure 4e), indicating improved fidelity for wider features. This trend confirms that inkjet printing offers enhanced control and precision for larger conductor patterns. The same inkjet strategy supports rapid, scalable fabrication of high-resolution, versatile patterned stretchable conductors (Figure 4f–h) and compatibility with a wide range of substrate materials (Figure S17). These attributes provide a robust foundation for the integration of large-area stretchable electronic systems.

By co-engineering the strain-engineered substrate and stretchable conductors, we successfully developed a hybrid stretchable electronic system exhibiting outstanding electromechanical stability. The dimensions of the rigid island are intentionally designed to be slightly larger than those of the rigid component. This design ensures the effective isolation of the component from localized strain and enables robust integration with the stretchable electrodes. As shown in Figure S18a,b, LED chips embedded within the rigid islands of the gradient modulus substrate are interconnected via inkjet-printed stretchable conductors, enabling robust and stable performance under 30% uniaxial strain. The current remains within ±10% of the initial value under complex deformation modes, with no observable change in luminance (Figure S18c,d), confirming reliable current transmission and consistent optical output under mechanical stress. We further evaluated the durability of the device under tensile deformation. During short-term cyclic stretching, both the electrical response and the functional output of the LED remained stable. No significant performance degradation was observed, as shown in Figure S19. This demonstrates that the synergistic design of strain-isolated substrates and stretchable electrodes ensures system reliability under dynamic mechanical deformation. To further evaluate the protective effect of this hybrid strategy on rigid components, we compared the performance of LED devices integrated on conventional elastic substrates and on strain-engineered substrates. Under increasing strain, LEDs on the conventional substrate exhibited pronounced performance degradation, with a progressive drop in current and an abrupt failure at approximately 20% strain, indicative of electrical breakdown. In contrast, LEDs on the strain-isolated substrate maintained stable operation even at 40% strain, with negligible changes in current (Figure S20). This performance enhancement is attributed to the dual optimization of both substrate and conductor: the strain-engineered substrate effectively redistributes mechanical stress, reducing strain concentration at the rigid-soft interface, while the Ag-PDMS composite conductor provides strain-resilient electrical pathways, compensating for resistance fluctuations during deformation.

Building on the above demonstration of mechanical and electrical robustness, we further engineered a hybrid, stretchable, intelligent sensing system tailored for human motion monitoring. This system is capable of capturing multi-joint motion signals and transmitting them in real time to an external interface for analysis and recognition (Figure 5a). The system architecture leverages a co-designed strain-engineered substrate and heterogeneously integrated composite conductors to achieve functional segmentation and mechanical resilience. Specifically, regions of elevated modulus were patterned onto a PDMS substrate via ultraviolet lithography to serve as anchoring sites for rigid components. A micro-scale sensing network was subsequently constructed via DIW, ensuring high-resolution signal mapping (Figure S21). As depicted in Figure 5b, the sensing mechanism of the stretchable hybrid circuit involves a three-stage signal transduction process: mechanical strain induces resistance variation, which is initially captured by a high-precision resistive sensing module. This raw signal is then conditioned, amplified, and filtered through a custom-designed analog front-end (AFE) circuit. The resulting data are transmitted to the central control unit via a modular data acquisition interface. To achieve simultaneous strain sensing and signal transmission within a unified architecture, we employed two distinct Ag-PDMS composite formulations. A high-conductivity composite (65 wt.%) served as the stretchable interconnect electrode, offering negligible resistance fluctuation ($\Delta R/R_0 <$ 5%) even under 80% strain. In contrast, a low-conductivity composite (44 wt.%) was adopted as the strain-sensitive element, exhibiting a gauge factor greater than 50 at 60% strain. This material bifurcation enabled clear functional decoupling within the circuit (Figure 5c), facilitating concurrent signal acquisition and transmission without interference. Performance evaluation confirmed that the sensing units responded reliably across multiple mechanical deformation modes, including axial stretching (Figure S22a) and out-of-plane bending (Figure S22b). To mitigate signal crosstalk in dense circuit geometries, an additional PDMS insulation layer was incorporated to serve as a dielectric barrier at critical interconnect junctions. This configuration effectively prevented leakage and capacitive coupling at wire crossings, thereby preserving signal integrity and enhancing overall circuit reliability under complex operational conditions.

We examined the interfacial stability of the stretchable circuit under different deformation conditions (Figure 5d). The rigid chip, protected by the strain-engineered substrate, experiences minimal strain and remains reliably bonded to the substrate. Meanwhile, the sensing layer, sharing the same composition as the electrodes and substrate, maintains stable interfaces even under large deformations. To validate the system-level integration, we first conducted a comprehensive evaluation of the stretchable hybrid circuit configured with a single sensor node (Figure S23). The results demonstrated that the sensor node reliably captured biomechanical signals. Specifically, the strain sensor distinguished the flexion of the distal interphalangeal (DIP), proximal interphalangeal (PIP), and metacarpophalangeal (MCP) joints with high fidelity. Furthermore, the circuit resolved the resistance changes corresponding to each of the five MCP

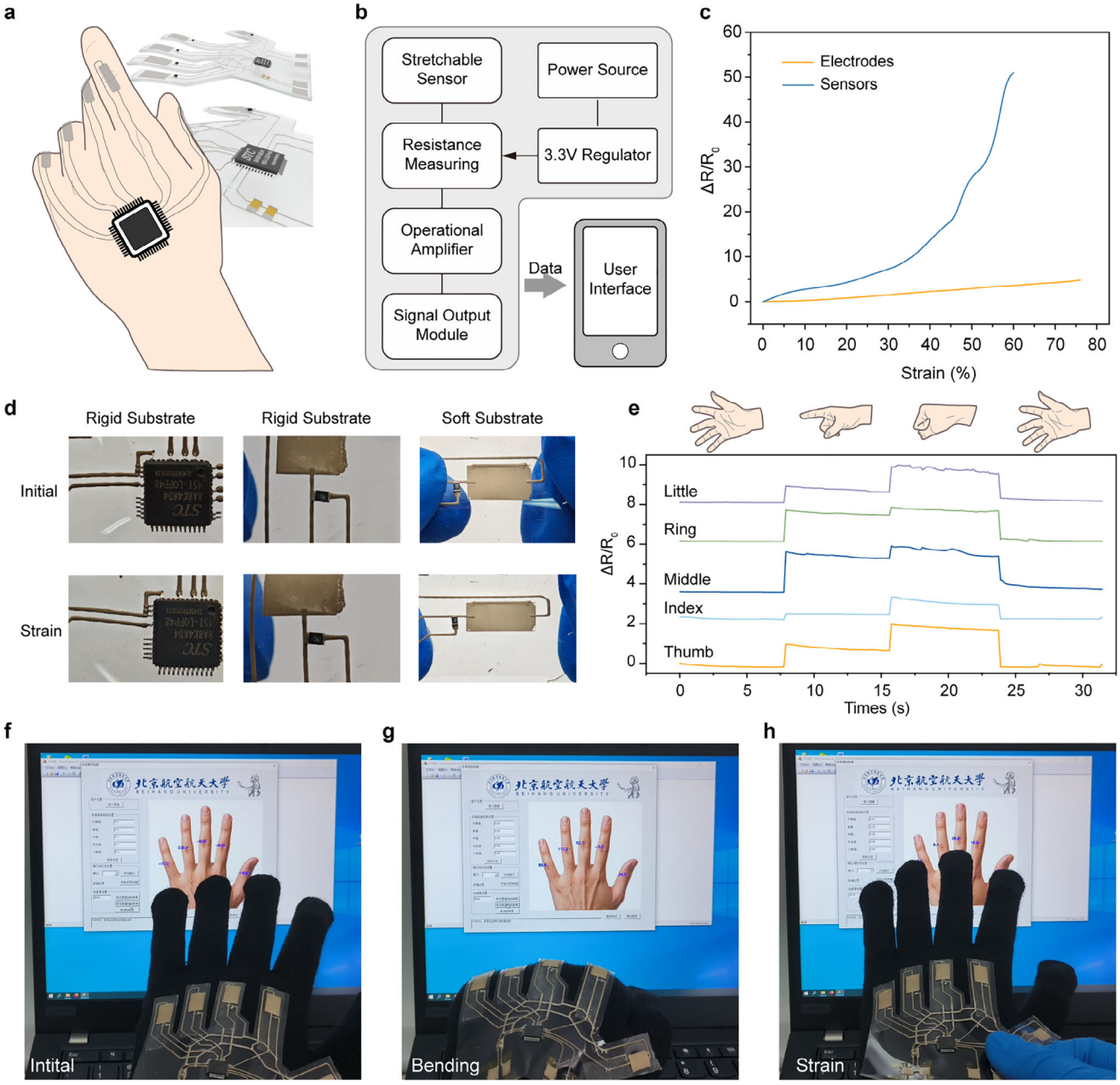

FIGURE 5 | Applications of stretchable hybrid circuits for gesture recognition. (a) Schematic illustration of a stretchable hybrid circuit applied for finger joint motion detection. (b) Workflow of gesture recognition, including signal acquisition, data processing, and transmission. (c) Electrical response of sensors and electrodes under mechanical strain. (d) Interfacial stability of the stretchable circuit under deformation. (e) Signal variation of the MCP joint under different gesture states. (f) Integrated system for real-time finger movement recognition. (g) Representative signals generated during a full fist gesture. (h) The system maintains a stable signal output during continuous stretching, demonstrating mechanical and electrical robustness.

joints during various hand gestures (Figure 5e), providing a foundation for subsequent machine-learning-based pattern recognition. Real-time tracking of finger joint bending angles was achieved via continuous signal acquisition and mapping to a visual interface (Figure 5f). Through the extraction of key features from different joint-angle combinations, the system enabled accurate classification of complex hand gestures (Figure 5g). Importantly, mechanical reliability tests revealed stable signal acquisition and uninterrupted data transmission under substantial tensile strain applied directly to the chip module (Figure 5h). These results underscore the high electromechanical robustness of the substrate conductor co-design, affirming the system's potential for practical deployment in next-generation wearable electronics.

3 | Conclusions

We present a synergistically designed stretchable hybrid electronic system that combines a strain-isolated substrate, multifunctional conductive composites, and a high-resolution fabrication approach to ensure reliable electromechanical performance under complex deformation conditions. Through photochemically induced gradient crosslinking, we spatially modulated the

mechanical properties of PDMS substrates, achieving up to an 11-fold variation in Young's modulus. This strain-engineered substrate effectively mitigates stress concentration around rigid electronic components, thereby supporting their stable operation under large tensile strains. To address the need for both conductivity and sensitivity, we formulated composite conductive materials by tuning the silver particle concentration within a PDMS matrix. High-concentration composites (65 wt.%) offer low-impedance conduction pathways, while low-concentration composites (44 wt.%) exhibit pronounced sensitivity to mechanical deformation, enabling dual functionality in signal transmission and strain sensing. Using inkjet printing, we patterned these materials into well-defined circuit architectures with excellent uniformity and resolution, demonstrating the feasibility of scalable, high-precision integration. Built on this platform, we developed a wearable stretchable circuit capable of high-fidelity monitoring of multi-joint finger movements. The integrated system achieves stable signal acquisition, amplification, and transmission during dynamic deformation, enabling real-time recognition of complex hand gestures by continuously mapping joint motion to a digital interface. Collectively, these results demonstrate the potential of our approach to enable next-generation wearable electronics, particularly for applications in electronic skin and human-machine interfaces that require clinically relevant motion-tracking performance. Although wearable motion monitoring technologies have demonstrated encouraging performance, several aspects still require further optimization. The current spatial resolution is constrained by the sensor layout and interconnect density, which could be enhanced by reducing device dimensions and increasing array integration density. By integrating the proposed wearable sensing system with low-power signal acquisition architectures and wireless data transmission schemes, the platform is expected to facilitate fully untethered operation. Such advancements will allow the system to be extended toward a broader range of applications, including long-term health monitoring and intuitive human–machine interfaces, where seamless integration and continuous data flow are paramount.

4 | Experimental Section

4.1 | Fabrication of the Strain-Engineered Substrate

To prepare the strain-engineered substrate, polydimethylsiloxane (PDMS; Sylgard 184, Dow Corning) was mixed at a base-to-crosslinker weight ratio of 5:1. Benzophenone (BP; Aladdin, 99.5%) was first dissolved in xylene (Innochem, analytical grade, 99%) at a mass ratio of 1:2. The resulting BP solution was then blended with the PDMS precursor at a base-to-BP weight ratio of 50:1. The mixture was stirred using a magnetic stirrer at 200 rpm for 15 min in the absence of light to prevent premature activation. Subsequently, a thin film of the BP-PDMS mixture (approximately 5 g per 10 × 10 cm area) was spin-coated onto a glass substrate pre-coated with a water-soluble sacrificial layer composed of 10 wt.% dextran solution (Innochem) in deionized water. The coated film was selectively exposed to ultraviolet light (365 nm) through a photomask at an intensity of 28.90 mW/cm^2 for 60 min to induce spatially controlled photochemical crosslinking. Following UV exposure, the substrate was thermally cured in an oven at 80°C for 3 h and subsequently released in water to dissolve the sacrificial layer and retrieve the patterned PDMS film.

4.2 | Fabrication of the Stretchable Conductors

Silver nanoparticles (10 μm, Sigma-Aldrich) were first dispersed in methyl isobutyl ketone (MIBK, Innochem, 99.5%) at a mass ratio of 3:1 and stirred at 150 rpm for 30 min to ensure uniform dispersion. Separately, a PDMS precursor was prepared by mixing the base and curing agent (Sylgard 184, Dow Corning) at a mass ratio of 10:1 and stirred for 10 min. The premixed PDMS was then added to the silver dispersion and gently stirred for an additional 10 min to obtain a homogeneous composite ink. The final mass ratio of Ag nanoparticles, MIBK, and PDMS was controlled at 3:1.1:1. This composition was optimized to ensure full dispersion of silver particles without agglomeration, while maintaining appropriate rheological properties for printing. The resulting ink was subsequently printed onto the prefabricated substrate using a direct-writing technique. After printing, the patterned electrodes were annealed on a hot plate at 100°C for 4 h to facilitate slow solvent evaporation and complete curing of the composite matrix, thereby forming stretchable conductive traces with stable mechanical and electrical properties.

4.3 | Fabrication of Stretchable Circuit

The stretchable circuit was constructed by integrating a strain-isolation substrate with patterned stretchable conductors. First, the UV-modified substrate from Section 4.1 was used as the mechanical and chemical platform. Conductive pathways were patterned on the substrate via inkjet printing using the silver-based ink developed in Section 4.2. Rigid electronic components, including chips and surface-mounted devices (SMDs), were then positioned and bonded onto predefined rigid island regions within the substrate. To ensure electrical insulation at intersections of conductive traces, a thin layer of PDMS was selectively applied as an insulating barrier. A second layer of conductive traces was then printed at designated locations using the same inkjet process, allowing vertical interconnects and completing the multi-layer circuit architecture.

Acknowledgements

The authors thank the support of the National Natural Science Foundation of China (Nos. 62422120, 52371202, 52192610, 52572153, 52203307, 52125205, 52532005, and 52250398), the Natural Science Foundation of Beijing (L223006), National Key Research and Development (R&D) Program from Ministry of Science and Technology of China (2024YFB3814100) and the Fundamental Research Funds for the Central Universities for their support. The authors also thank Xuzhou B&C Chemical Co. Ltd. for providing the photoresist (HTA116, HTA112, B&C Chemicals) used in our work.

Conflicts of Interest

The authors declare no conflicts of interest.

Data Availability Statement

The data that support the findings of this study are available from the corresponding author upon reasonable request.

References

1. N. Sun, Q. Rong, J. Wu, et al., "Fully Printable Integrated Multifunctional Sensor Arrays for Intelligent Lithium-Ion Batteries," *Nature Communications* 16 (2025): 7361, https://doi.org/10.1038/s41467-025-62657-2.

2. Y. Luo, M. R. Abidian, J.-H. Ahn, et al., "Technology Roadmap for Flexible Sensors," *ACS Nano* 17 (2023): 5211–5295, https://doi.org/10.1021/acsnano.2c12606.

3. M. Hassan, G. Abbas, N. Li, et al., "Significance of Flexible Substrates for Wearable and Implantable Devices: Recent Advances and Perspectives," *Advanced Materials Technologies* 7 (2022): 2100773, https://doi.org/10.1002/admt.202100773.

4. Z. Xu, X. Pan, H. Lu, et al., "Surface Energy-Assisted Patterning of Vapor Deposited All-Inorganic Perovskite Arrays for Wearable Optoelectronics," *Advanced Science* 11 (2024): 2402635, https://doi.org/10.1002/advs.202402635.

5. Y. Lu, X. Qu, W. Zhao, et al., "Highly Stretchable, Elastic, and Sensitive MXene-Based Hydrogel for Flexible Strain and Pressure Sensors," *Research* 2020 (2020): 2038560.

6. G. Ge, W. Yuan, W. Zhao, et al., "Highly Stretchable and Autonomously Healable Epidermal Sensor Based on Multi-Functional Hydrogel Frameworks," *Journal of Materials Chemistry A* 7 (2019): 5949–5956, https://doi.org/10.1039/C9TA00641A.

7. K. Zhou, Y. Zhao, X. Sun, et al., "Ultra-Stretchable Triboelectric Nanogenerator as High-Sensitive and Self-Powered Electronic Skins for Energy Harvesting and Tactile Sensing," *Nano Energy* 70 (2020): 104546, https://doi.org/10.1016/j.nanoen.2020.104546.

8. G. Ge, Y. Lu, X. Qu, et al., "Muscle-Inspired Self-Healing Hydrogels for Strain and Temperature Sensor," *ACS Nano* 14 (2020): 218–228, https://doi.org/10.1021/acsnano.9b07874.

9. Y. Zhao, W. Gao, K. Dai, et al., "Bioinspired Multifunctional Photonic-Electronic Smart Skin for Ultrasensitive Health Monitoring, for Visual and Self-Powered Sensing," *Advanced Materials* 33 (2021): 2102332, https://doi.org/10.1002/adma.202102332.

10. Y. Xia, Y. Zhu, X. Zhi, et al., "Transparent Self-Healing Anti-Freezing Ionogel for Monolayered Triboelectric Nanogenerator and Electromagnetic Energy-Based Touch Panel," *Advanced Materials* 36 (2024): 2308424, https://doi.org/10.1002/adma.202308424.

11. J. He, R. Wei, S. Ge, et al., "Artificial Visual-Tactile Perception Array for Enhanced Memory and Neuromorphic Computations," *InfoMat* 6 (2024): 12493.

12. R. Bao, J. Tao, J. Zhao, M. Dong, J. Li, and C. Pan, "Integrated Intelligent Tactile System for a Humanoid Robot," *Science Bulletin* 68 (2023): 1027–1037.

13. X. Wang, H. Zhang, L. Dong, et al., "Self-Powered High-Resolution and Pressure-Sensitive Triboelectric Sensor Matrix for Real-Time Tactile Mapping," *Advanced Materials* 28 (2016): 2896–2903, https://doi.org/10.1002/adma.201503407.

14. W. Yang, S. Liu, Z. Wang, et al., "Bioinspired Composite Fiber Aerogel Pressure Sensor for Machine-Learning-Assisted Human Activity and Gesture Recognition," *Nano Energy* 127 (2024): 109799, https://doi.org/10.1016/j.nanoen.2024.109799.

15. L. Tang, H. Wang, J. Ren, and X. Jiang, "Highly Robust Soft-Rigid Connections via Mechanical Interlocking for Assembling Ultra-Stretchable Displays," *npj Flexible Electronics* 8 (2024): 50, https://doi.org/10.1038/s41528-024-00337-9.

16. H. Yoon, S. Jeong, B. Lee, and Y. Hong, "A Site-Selective Integration Strategy for Microdevices on Conformable Substrates," *Nature Electronics* 7 (2024): 383–395, https://doi.org/10.1038/s41928-024-01159-3.

17. Z. Yang, S. Huo, Z. Zhang, et al., "High-Precision Multibit Opto-Electronic Synapses Based on ReS_2/h-BN/Graphene Heterostructure for Energy-Efficient and High-Accuracy Neuromorphic Computing," *Advanced Functional Materials* 35 (2025): 2509119, https://doi.org/10.1002/adfm.202509119.

18. H. Cho, B. Lee, D. Jang, J. Yoon, S. Chung, and Y. Hong, "Recent Progress in Strain-Engineered Elastic Platforms for Stretchable Thin-Film Devices," *Materials Horizons* 9 (2022): 2053–2075, https://doi.org/10.1039/D2MH00470D.

19. M. Cai, S. Nie, Y. Du, C. Wang, and J. Song, "Soft Elastomers With Programmable Stiffness as Strain-Isolating Substrates for Stretchable Electronics," *ACS Applied Materials & Interfaces* 11 (2019): 14340–14346, https://doi.org/10.1021/acsami.9b01551.

20. W. Wang, S. Wang, R. Rastak, et al., "Strain-Insensitive Intrinsically Stretchable Transistors and Circuits," *Nature Electronics* 4 (2021): 143–150.

21. X. Pan, Z. Xu, R. Bao, and C. Pan, "Research Progress in Stretchable Circuits: Materials, Methods, and Applications," *Advanced Sensor Research* 2 (2023): 2300065, https://doi.org/10.1002/adsr.202300065.

22. J. Lee, J. Wu, J. H. Ryu, et al., "Stretchable Semiconductor Technologies With High Areal Coverages and Strain-Limiting Behavior: Demonstration in High-Efficiency Dual-Junction GaInP/GaAs Photovoltaics," *Small* 8 (2012): 1851–1856, https://doi.org/10.1002/smll.201102437.

23. D. Lee, S.-B. Kim, T. Kim, et al., "Stretchable OLEDs Based on a Hidden Active Area for High Fill Factor and Resolution Compensation," *Nature Communications* 15 (2024): 4349, https://doi.org/10.1038/s41467-024-48396-w.

24. J. Li, X. Pan, Y. Zhang, et al., "Ultrathin Breathable and Stretchable Electronics Based on Patterned Nanofiber Composite Network," *Materials Today Nano* 23 (2023): 100359, https://doi.org/10.1016/j.mtnano.2023.100359.

25. D. H. Lee, J. Yea, J. Ha, et al., "Rugged Island-Bridge Inorganic Electronics Mounted on Locally Strain-Isolated Substrates," *ACS Nano* 18 (2024): 13061–13072, https://doi.org/10.1021/acsnano.4c01759.

26. Y. Shao, J. Yan, Y. Zhi, et al., "A Universal Packaging Substrate for Mechanically Stable Assembly of Stretchable Electronics," *Nature Communications* 15 (2024): 6106, https://doi.org/10.1038/s41467-024-50494-8.

27. Y. Xia, T. Zhu, K. Chen, et al., "Fatigue-Resistant Metal-Film-Based Flexible Conductors With A Coherent Gradient Nanolayered Architecture," *Nature Electronics* 9 (2026): 33–44.

28. G. Wang, G. Ghosh, M. Park, and N.-E. Lee, "Highly Stretchable and Mechanically Robust Copolymer-Based Strain-Engineered Substrate for Wearable Electronics," *Chemical Engineering Journal* 499 (2024): 156471, https://doi.org/10.1016/j.cej.2024.156471.

29. J. He, J. Huang, R. Li, et al., "Hysteresis-Free And Dynamically Resilient Strain Sensor Enabled By Interfacial Coordination," *Science Advances* 12 (2026): aea2450.

30. H.-G. Park, M. Kim, H. Park, and J. H. Oh, "Synthesis of a Photo-Crosslinkable Elastomer for Stretchable Electronics and Its Use in Strain-Insensitive Pressure Sensors," *Advanced Functional Materials* 34 (2024): 2312034, https://doi.org/10.1002/adfm.202312034.

31. X. Liu, Q. Wang, S. Zhou, et al., "Stiffness and Interface Engineered Soft Electronics With Large-Scale Robust Deformability," *Advanced Materials* 36 (2024): 2407886, https://doi.org/10.1002/adma.202407886.

32. X. Pan, J. Li, Z. Xu, et al., "A High Stretchability Micro-Crack Tactile Sensor System Based on Strain-Isolation Substrate," *Materials Today Physics* 48 (2024): 101562.

33. B. Sun, Z. Li, Z. Song, et al., "Gradient Modulus Strategy for Alleviating Stretchable Electronic Strain Concentration," *Advanced Functional Materials* 34 (2024): 2410676, https://doi.org/10.1002/adfm.202410676.

34. M. Kim, S. Hong, J. J. Park, et al., "A Gradient Stiffness-Programmed Circuit Board by Spatially Controlled Phase-Transition of Supercooled Hydrogel for Stretchable Electronics Integration," *Advanced Materials* 36 (2024): 2313344, https://doi.org/10.1002/adma.202313344.

35. Z. He, B. Sun, H. Lu, et al., "Focus-Tunable Real-Time Imaging System Based on Ultrathin Perovskite Curved Image Sensor with Hierarchical Mesh Design," *Science Advances* 11 (2025): adw7826.

36. Z. Chen, R. Zhou, J. Huang, et al., "Strain-Insensitive Pre-Stretch-Stabilized Polymer/Gold Hybrid Electrodes for Electrochemiluminescent Devices," *Advanced Functional Materials* 34 (2024): 2406434, https://doi.org/10.1002/adfm.202406434.

37. X. Li, C. Chen, Z. Li, et al., "Inter-Skeleton Conductive Routes Tuning Multifunctional Conductive Foam for Electromagnetic Interference Shielding, Sensing and Thermal Management," *Nano-Micro Letters* 17 (2024): 52, https://doi.org/10.1007/s40820-024-01540-z.

38. J. Jang, H. Choo, S. Lee, et al., "Reconfigurable Assembly of Self-Healing Stretchable Transistors and Circuits for Integrated Systems," *Nature Electronics* 8 (2025): 474–484, https://doi.org/10.1038/s41928-025-01389-z.

39. W. Babatain, "Rapid Interconnects for 3D Soft Electronics," *Nature Electronics* 7 (2024): 950–951, https://doi.org/10.1038/s41928-024-01282-1.

40. H.-C. Xu, Y. Liu, Y.-P. Mo, et al., "All-Fiber Anti-Jamming Capacitive Pressure Sensors Based on Liquid Metals," *Rare Metals* 44 (2025): 4839–4850.

41. Z. Guan, Y. Jiang, Y. Zhou, et al., "Liquid Metal-Based Electrodes for Flexible Electronics," *Rare Metals* 44 (2025): 6897–6923, https://doi.org/10.1007/s12598-025-03466-w.

42. M. Qi, R. Yang, Z. Wang, et al., "Bioinspired Self-healing Soft Electronics," *Advanced Functional Materials* 33 (2023): 2214479, https://doi.org/10.1002/adfm.202214479.

43. Y. Qi, B. Tan, R. Zhu, D. Li, S. Liu, and X. Chen, "Liquid Metal Composites for Wearable Healthcare Sensors," *Rare Metals* 44 (2025): 5980–6001, https://doi.org/10.1007/s12598-025-03335-6.

44. X. Liu, W. Zhang, X. Zhang, et al., "Transparent Ultrahigh-Molecular-Weight Polyethylene/MXene Films with Efficient UV-Absorption for Thermal Management," *Nature Communications* 15 (2024): 3076, https://doi.org/10.1038/s41467-024-47432-z.

45. H. Liu, Q. Li, Y. Bu, et al., "Stretchable Conductive Nonwoven Fabrics with Self-Cleaning Capability for Tunable Wearable Strain Sensor," *Nano Energy* 66 (2019): 104143, https://doi.org/10.1016/j.nanoen.2019.104143.

46. J. He, S. Wang, R. Han, et al., "Wide Detection Range Flexible Pressure Sensors Based on 3D Interlocking Structure TPU/ZnO NWs," *Advanced Functional Materials* 35 (2025): 2418791, https://doi.org/10.1002/adfm.202418791.

47. Y. Liu, J. Tao, Y. Mo, R. Bao, and C. Pan, "Ultrasensitive Touch Sensor for Simultaneous Tactile and Slip Sensing," *Advanced Materials* 36 (2024): 2313857, https://doi.org/10.1002/adma.202313857.

48. R. Han, Y. Liu, Y. Mo, et al., "High Anti-Jamming Flexible Capacitive Pressure Sensors Based on Core–Shell Structured AgNWs@TiO_2," *Advanced Functional Materials* 33 (2023): 2305531, https://doi.org/10.1002/adfm.202305531.

49. W. Yang, H. Liu, H. Du, et al., "Robust and Superelastic Spider Web-Like Polyimide Fiber-Based Conductive Composite Aerogel for Extreme Temperature-Tolerant Linear Pressure Sensor," *Science China Materials* 66 (2023): 2829–2842, https://doi.org/10.1007/s40843-022-2418-1.

50. Z. Xu, X. Han, W. Wu, et al., "Controlled On-Chip Fabrication of Large-Scale Perovskite Single Crystal Arrays for High-Performance Laser and Photodetector Integration," *Light Science & Applications* 12 (2023): 67.

51. Q. Zhuang, K. Yao, C. Zhang, et al., "Permeable, Three-Dimensional Integrated Electronic Skins with Stretchable Hybrid Liquid Metal Solders," *Nature Electronics* 7 (2024): 598–609, https://doi.org/10.1038/s41928-024-01189-x.

52. W. Zhu, R. Li, X. Liu, et al., "Photophysical Properties of Copper Halides With Strongly Confined Excitons and Their High-Performance X-Ray Imaging," *Advanced Functional Materials* 34 (2024): 2316449, https://doi.org/10.1002/adfm.202316449.

53. Y. Jiao, R. Li, H. Wang, et al., "Bright and Fast-Response Hybrid X-Ray Scintillators by Molecular and Dielectric Confinement," *Angewandte Chemie International Edition* 64 (2025): 202504576, https://doi.org/10.1002/anie.202504576.

54. T. Wang, Q. Liu, H. Liu, B. Xu, and H. Xu, "Printable and Highly Stretchable Viscoelastic Conductors With Kinematically Reconstructed Conductive Pathways," *Advanced Materials* 34 (2022): 2202418, https://doi.org/10.1002/adma.202202418.

55. N. Matsuhisa, M. Kaltenbrunner, T. Yokota, et al., "Printable Elastic Conductors with a High Conductivity for Electronic Textile Applications," *Nature Communications* 6 (2015): 7461, https://doi.org/10.1038/ncomms8461.

56. D. Suh, K. P. Faseela, W. Kim, et al., "Electron Tunneling of Hierarchically Structured Silver Nanosatellite Particles for Highly Conductive Healable Nanocomposites," *Nature Communications* 11 (2020): 2252, https://doi.org/10.1038/s41467-020-15709-8.

57. H. Huang, H. Wang, D. Wang, et al., "Emitter Orientation-Dependent Copper Halide Scintillators for High Resolution X-Ray Imaging," *Chemical Engineering Journal* 523 (2025): 168845, https://doi.org/10.1016/j.cej.2025.168845.

58. H. Ma, C. Liu, Z. Yang, et al., "Programmable and Flexible Wood-Based Origami Electronics," *Nature Communications* 15 (2024): 9272, https://doi.org/10.1038/s41467-024-53708-1.

59. K. Tian, J. Jing, M. Wen, et al., "Designing Functional Filler Networks via In Situ Silver Nanoparticles Through Barrier Tuning and Volume Exclusion," *Nature Communications* 17 (2025): 728.

60. J. Choi, H. Nam, D. Park, et al., "Room-Temperature, High-Resolution Soft Anisotropic Conductive Film for Electrical Interfacing in Stretchable Electronics," *Advanced Functional Materials* 36 (2025): 16217.

Supporting Information

Additional supporting information can be found online in the Supporting Information section.

Supporting File: adfm75046-sup-0001-SuppMat.docx.